

# Measurement of Dicke Narrowing in Electromagnetically Induced Transparency

M. Shuker,<sup>1</sup> O. Firstenberg,<sup>1</sup> R. Pugatch,<sup>2</sup> A. Ben-Kish,<sup>1</sup> A. Ron,<sup>1</sup> and N. Davidson<sup>2</sup>

<sup>1</sup>*Department of Physics, Technion-Israel Institute of Technology, Haifa 32000, Israel*

<sup>2</sup>*Department of Physics of Complex Systems, Weizmann Institute of Science, Rehovot 76100, Israel*

Dicke narrowing is a phenomena that dramatically reduces the Doppler width of spectral lines, due to frequent velocity-changing collisions. A similar phenomena occurs for electromagnetically induced transparency (EIT) resonances, and facilitates ultra-narrow spectral features in room-temperature vapor. We directly measure the Dicke-like narrowing by studying EIT line-shapes as a function of the angle between the pump and the probe beams. The measurements are in good agreement with an analytic theory with no fit parameters. The results show that Dicke narrowing can increase substantially the tolerance of hot-vapor EIT to angular deviations. We demonstrate the importance of this effect for applications such as imaging and spatial solitons using a single-shot imaging experiment, and discuss the implications on the feasibility of storing images in atomic vapor.

Dicke narrowing [1] is a phenomenon in which the width of Doppler-broadened absorption lines is dramatically reduced due to frequent velocity-changing collisions. The narrowing factor is proportional to the mean free-path between collisions divided by the radiation wavelength. This leads, for example, to ultra-narrow microwave absorption lines in wall-coated cells [2, 3].

Electromagnetically induced transparency (EIT) involves two radiation fields, a probe and a pump, and may also exhibit Doppler broadening if the wave-vectors of the radiation fields,  $\mathbf{q}_1$  and  $\mathbf{q}_2$ , are not equal. As an example we consider the EIT resonance within the clock transition of an Alkali atom, imposing a frequency difference of several GHz between the two radiation fields. In this case there is a small difference in the Doppler shifts of the two fields, so we expect a residual Doppler broadening of the EIT resonance, given by  $\Gamma_D^{\text{res}} = |\mathbf{q}_1 - \mathbf{q}_2| v_{\text{th}}$ , where  $v_{\text{th}}$  is the one-dimensional mean thermal velocity of the atoms. However, in vapor cells with buffer-gas the measured resonances widths ( $\sim 100$  Hz) are far narrower than the expected broadening ( $\Gamma_D^{\text{res}} \simeq 10$  kHz). It has been commonly suggested to attribute this narrowing to a Dicke-like effect owing to collisions with the buffer gas [4, 5, 6, 7], but no measurement of a finite Dicke-narrowed width of an EIT line was performed. Recently we developed an analytic theory [8] and showed that the Dicke-like narrowing factor for an EIT resonance is proportional to the mean free-path divided by the wavelength associated with the *wave-vectors difference*  $\lambda_{\text{EIT}} = 2\pi/|\mathbf{q}_1 - \mathbf{q}_2|$ . Typically for a clock-transition EIT setup the residual Doppler broadening is suppressed by Dicke narrowing to  $\sim 1$  Hz, negligible compared to other broadening mechanisms and therefore not measurable.

In order to verify our theoretical prediction, we investigate a degenerate EIT scheme ( $|\mathbf{q}_1| = |\mathbf{q}_2|$ ) and introduce a small angular deviation between the pump and the probe. By controlling the angular deviation the Dicke-Doppler width can be increased to a measurable level and compared with the theory. We present two different types of experiments: a spectroscopic measure-

ment of EIT line-shapes for various deviation angles and a single-shot imaging measurement of a divergent probe. The angular deviation is used here as a tool to study the effect of Dicke narrowing, but it has important influence on several possible applications of EIT where the angular deviation (or divergence) is unavoidable. Those include slowing and storing of images [9], solitons [10, 11], and strong confinement [12].

Several authors have previously considered the effect of angular deviation between the pump and the probe. In [13] the measured width of the EIT lines was found to be far below the broadening expected from the angular deviations in the setup. In [14] and [15] a broadening of several MHz due to an angular deviation of several mrad was measured. All these experiments were performed in cells with no buffer gas, showing only the residual Doppler broadening and not the Dicke narrowing.

In [8] we calculated the energy absorption spectrum of the probe beam in a  $\Lambda$ -type EIT system, in the regime of a weak probe and low power-broadening. The EIT line-shape is obtained on-top of the single photon absorption spectrum, and we consider the case where the one-photon transition is Doppler broadened while the two photon transition is Dicke narrowed. This is the case for most of the realistic EIT experiments in buffer gas cells since the optical wavelength ( $\lambda \simeq 1 \mu\text{m}$ ) is much smaller than the wavelength associated with the wave-vectors difference ( $\lambda_{\text{EIT}} = 1 - 10 \text{ cm}$ ), and the mean free-path between collisions,  $L$ , is usually in between (i.e.  $\lambda < L < \lambda_{\text{EIT}}$ ). For this case we derived the expression [8]

$$S_2 = \frac{-|\Omega_2|^2}{[\Gamma + \mathbf{q}_1(\mathbf{q}_1 - \mathbf{q}_2)v_{\text{th}}^2/\gamma]^2} \times \frac{\Gamma_{12} + \eta\Gamma_D^{\text{res}}}{\Delta_R^2 + [\Gamma_{12} + \eta\Gamma_D^{\text{res}}]^2}, \quad (1)$$

where  $S_2(\Delta_R)$  is the two-photon absorption spectrum,  $\Delta_R$  is the Raman detuning,  $\Omega_2$  is the Rabi frequency of the pump,  $\Gamma$  is the optical decoherence rate,  $\gamma$  is the collisions rate,  $\Gamma_{21}$  is the ground state decoherence rate and  $\eta$  is the EIT-Dicke narrowing factor, given by  $\eta = \Gamma_D^{\text{res}}/\gamma = 2\pi(L/\lambda_{\text{EIT}})$ . Note that Eq. (1) is valid for the case of small one-photon detuning and de-

pends only on the Raman detuning  $\Delta_R$ . In our experiment we use small angular deviation,  $\theta \leq 1$  mrad, between the pump and the probe, and a nearly degenerate  $\Lambda$  system. For that case  $|\mathbf{q}_1 - \mathbf{q}_2| = q\theta$ , where  $q = |\mathbf{q}_1| = |\mathbf{q}_2|$ . Therefore both the residual Doppler broadening,  $\Gamma_D^{\text{res}} = |\mathbf{q}_1 - \mathbf{q}_2| v_{\text{th}} = q\theta v_{\text{th}}$ , and the EIT-Dicke narrowing factor,  $\eta = q\theta v_{\text{th}}/\gamma = 2\pi\theta(L/\lambda)$ , are linear in  $\theta$ . Finally the EIT line-shape can be written as

$$S_2(\Delta_R) = \frac{-|\Omega_2|^2}{[\Gamma + \frac{2\pi L}{\lambda}\Gamma_D\theta^2]^2} \times \frac{\Gamma_{12} + \frac{2\pi L}{\lambda}\Gamma_D\theta^2}{\Delta_R^2 + [\Gamma_{12} + \frac{2\pi L}{\lambda}\Gamma_D\theta^2]^2}, \quad (2)$$

where  $\Gamma_D = qv_{\text{th}}$  is the one-photon Doppler width. We find that the EIT resonance has the shape of a Lorentzian with an excess width, over the width at  $\theta = 0$ , of

$$\eta\Gamma_D^{\text{res}} = \frac{2\pi L}{\lambda}\Gamma_D\theta^2. \quad (3)$$

This implies that the excess width will be *quadratic* in the angular deviation, unlike regular Doppler width which has a linear dependence.

In the first experiment we measure the EIT resonances for different angular deviations between the pump and the probe. The EIT is performed within the D1 transition of  $^{87}\text{Rb}$  (Fig. 1.a). Two Zeeman sub-levels of the ground state ( $|F = 2; m_F = 0\rangle, |F = 2; m_F = +2\rangle$ ) are used as the two lower levels of a nearly-degenerate  $\Lambda$ -system. The experimental setup is depicted in Fig. 1.b. A vertical-cavity surface-emitting diode laser (VCSEL) is stabilized to the  $F = 2 \rightarrow F' = 1$  transition. The laser is split into two beams of perpendicular polarization, the pump and the probe, using a polarizing beam-splitter (PBS). The beams pass through acousto-optic modulators (AOM) allowing us to precisely control the Raman detuning. The pump and the probe are recombined on a second PBS, and co-propagate towards the vapor cell. A quarter wave-plate before the cell converts the pump and the probe polarizations to  $\sigma^+$  and  $\sigma^-$  respectively. The pump beam has a waist radius of  $w_{\text{pump}} = 2.3$  mm and a total intensity of  $180 \mu\text{W}$ . The pump power is selected so that the power-broadening due to the pump is small compared to the EIT natural homogeneous width ( $\Omega_2^2/\Gamma < \Gamma_{12}$ ). This ensures the low power-broadening assumed by our theoretical model. The probe beam has a waist radius of  $w_0 = 660 \mu\text{m}$  and its intensity is  $1 \mu\text{W}$ , much weaker than the pump. The small size of the probe guarantees that it experiences a nearly constant pump intensity. The waist of both beams is approximately at the middle of the vapor cell, making the angular *divergence* negligible. The angular deviation between the pump and the probe is precisely controlled by two mirrors, while keeping the probe concentric with the pump at the middle of the cell (see Fig. 1.c). The maximal translation of the probe at the edges of the cell, and at maximum angular deviation is  $\sim 25 \mu\text{m}$ , much smaller than the waist radius of the pump. We use a 5 cm long vapor cell

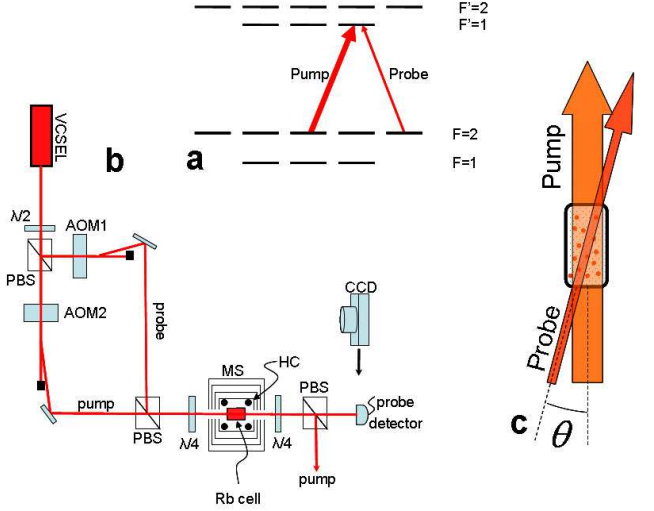


FIG. 1: (Color online) (a) Energy levels scheme of the D1 transition and the  $\Lambda$ -system used for the EIT. (b) The experimental setup: VCSEL - vertical cavity surface emitting laser diode.  $\lambda/2$  - half wave-plate. PBS - polarizing beam splitter. AOM - acousto-optic modulator.  $\lambda/4$  - quarter wave-plate. MS - magnetic shield. HC - Helmholtz coils. CCD - camera used for the imaging experiment. (c) Geometry of pump and probe beams crossing the vapor cell. A small angle between the beams,  $\theta$ , is introduced while keeping the beams concentric at the middle of the cell.

containing isotopically pure  $^{87}\text{Rb}$  and 10 Torr of Neon buffer gas. The temperature of the cell is  $\sim 52^\circ \text{C}$ , providing a Rubidium vapor density of  $\sim 1.3 \times 10^{11} / \text{cc}$ . The cell is placed within a four-layered magnetic shield, and a set of Helmholtz coils allows us to control the axial magnetic field. We use a small,  $B_z = 50 \text{ mG}$ , axial magnetic field to set the quantization axis. After the beams pass through the vapor cell they are separated using polarization optics, and the probe beam is measured by a photo-diode detector.

For each angular deviation we measure the EIT resonance by scanning the Raman detuning. The scan rate is slow enough to achieve the steady-state shape of the EIT resonance. Fig. 2 shows several EIT resonances measured for different angular deviations between the pump and the probe. As the angular deviation is increased the EIT resonance width increases and its amplitude decreases. The effect of angular deviation is indeed much smaller than one would expect from the residual Doppler width. For example, at an angular deviation of 0.5 mrad the expected residual Doppler width is  $\Gamma_D^{\text{res}} = 250 \text{ kHz}$  while the increase of the measured width (compared to that of perfect alignment) was only 2 kHz, showing dramatic Dicke-like narrowing. Note that the center of the EIT resonance is at non-zero Raman detuning due to a small light-shift [16].

To quantitatively verify our theory for Dicke narrowing

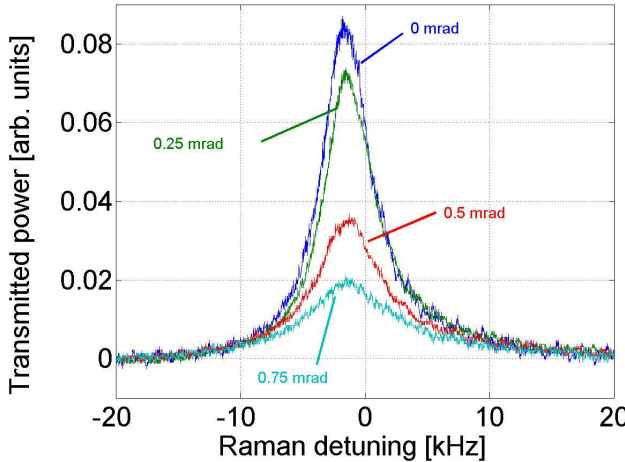


FIG. 2: (Color online) EIT resonances for several angular deviations between the pump and the probe. The angular deviation broadens the EIT line and reduces its amplitude.

of EIT resonances we compare the width and the amplitude of the experimental and theoretical EIT resonances. Fig. 3 depicts the measured full-width at half-maximum (FWHM) versus the angular deviation between the pump and the probe, as well as the theoretical curve. The quadratic dependence of the width on the angle is clearly evident from the experimental results — a distinct signature of the Dicke narrowing phenomenon, see Eq. (3). The calculation of the predicted excess width requires only three parameters: the one-photon Doppler width,  $\Gamma_D$ , the optical wavelength,  $\lambda$ , and the mean free-path between collisions,  $L$ . While both  $\Gamma_D$  and  $\lambda$  are known to a very good accuracy, a larger uncertainty exists in determining  $L$  since our medium involves two different species with different masses and densities. Following [7, 17] that discuss similar cases, the kinetic collision rate is given by  $r_{coll} = \frac{p}{k_B T} \sigma_k \bar{v}$  where  $p$  is the buffer gas pressure,  $T$  is the temperature,  $k_B$  is Boltzman's constant,  $\sigma_k$  is the kinetic cross-section for a collision between Ne and Rb and  $\bar{v}$  is the Ne-Rb mean relative velocity. The cross-section for collisions between Ne and Rb is given by  $\sigma_k = \pi R_{Rb-Ne}^2$ , where  $R_{Rb-Ne} \simeq 0.35$  nm is the hard-sphere radius [7, 18]. For our experimental conditions we get  $r_{coll} \simeq 8 \times 10^7$  collisions per second, and using the average thermal velocity of the Rb we find a mean free-path of  $L \simeq 2.2 \mu\text{m}$ . As seen in Fig 3, the agreement between the experimental data and the theory containing no fit parameters is very good.

Fig. 4 shows the peak transmission of the measured EIT resonance as a function of  $\theta$  (normalized to the peak transmission at  $\theta = 0$ ) together with the theoretical prediction of Eq. (2). The experimental measurements (circles) are denoted as a 'spectroscopic measurement'. The theoretical curve is plotted with the same parameters

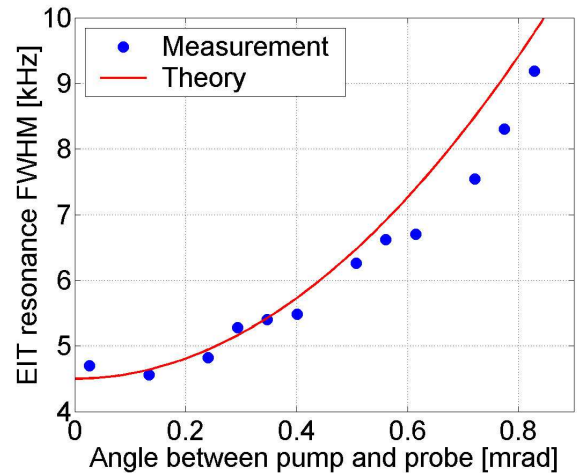


FIG. 3: (Color online) The FWHM of the EIT resonance vs. the angle between the pump and the probe. The theoretical curve was calculated with no fit parameters.

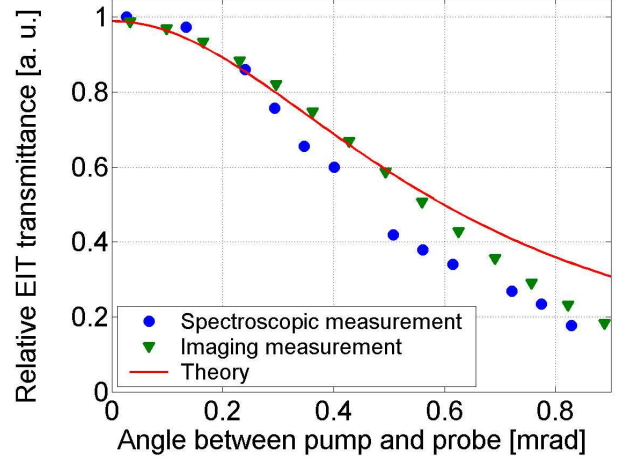


FIG. 4: (Color online) The relative amplitude of the EIT resonance vs. the angle between the pump and the probe, showing the agreement between a spectroscopic measurement (circles), a single-shot imaging measurement (triangles) and the theoretical model (solid line).

used in Fig. 3 and with  $\Gamma \simeq 150$  MHz (found from an absorption spectroscopy measurement). A good quantitative agreement between the theoretical model and the measurements is obtained, again with no fit parameters. The results presented in Figs. 3 and 4 confirm that Dicke-like narrowing is the dominant mechanism which determines the shape of EIT resonances at small angular deviations, and verify quantitatively the suggested model [8].

The effect of angular deviation on EIT is important for many applications related to the transverse properties of the probe beam, e.g. [19]. To demonstrate this

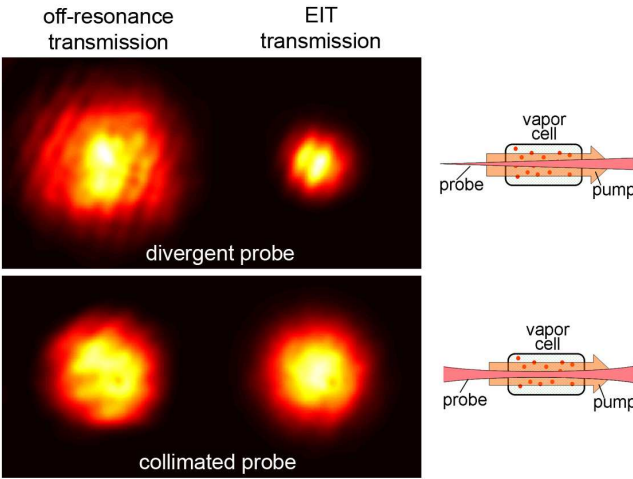


FIG. 5: (Color online) Single-shot imaging experiment, demonstrating the effect of angular divergence. The probe geometries are illustrated on the right. A divergent probe is strongly absorbed in its outer parts where the angular deviation is larger, while a collimated probe is almost not affected.

we study the beam shape of the transmitted probe by replacing the detector with a CCD camera (see Fig. 1.b) [20]. We set the Raman detuning to zero and compare the EIT transmission of a probe beam that is deliberately focused and diverges as it propagates towards the cell with that of a collimated probe beam. The angular deviation of the divergent probe is proportional to the radius,  $\theta(r) \propto r$ , with a maximal deviation of 1.9 mrad (at the waist-radius). The comparison between the off-resonance transmission (top-left image of Fig. 5) and EIT transmission (top-right image) demonstrates the effect of angular deviation on the divergent probe: the outer parts are strongly absorbed compared to the center, reducing the size of the EIT transmitted beam by more than 50% as compared to the off-resonance transmitted beam. The relative transparency as a function of the angular deviation can be found from the averaged radial cross-sections of these images, and it is plotted as triangles in Fig. 4 (denoted as ‘imaging measurement’). These results are in good agreement with the spectroscopic measurement. As a control experiment we reshape the probe as a collimated beam with a similar diameter (bottom part of Fig. 5). It is evident that in this case the sizes of the off-resonance and EIT transmitted beams are nearly identical (their size differs by less than 5%). This verifies that the divergent probe measurements are indeed related to the angular deviation.

In conclusion, we have measured the properties of EIT resonances as a function of the angular deviation ( $\theta$ ) between the pump and the probe, and compared the results to an analytic theory for Dicke-like narrowing in EIT. The measurements show that, in our buffer-gas cell, Doppler broadening due to the angular devia-

tion is strongly suppressed, and depends quadratically on  $\theta$  as opposed to the linear dependence for regular Doppler broadening. We found a very good quantitative agreement between the measurements and the theoretical model without any fit parameters. In a second experiment we demonstrated this effect in an imaging apparatus. The EIT transmission of a divergent probe beam is strongly affected by the large angular deviations at higher radii. In contrast, the collimated probe beam passes with nearly no distortion.

Dicke narrowing is a basic phenomenon that strongly affects the accuracy of EIT applications with non-degenerate lower levels, such as frequency references [21]. Dicke narrowing is also important for EIT applications where perfect alignment between the pump and the probe is not possible. These include experiments in which the divergence of the probe is inherently different from that of the pump - such as solitons [10, 11], imaging [9, 19] and strong confinement [12]. For example, considering storage of images in EIT medium, we find that the minimal feature size of the probe beam, assuming a planer pump beam, is limited by the associated angular divergence. Dicke narrowing in buffer-gas cells will increase substantially the acceptance angle of the EIT medium, compared to vacuum cells, and therefore enable storage of smaller feature sizes - i.e. higher resolution. The improvement depends on the exact experimental parameters, and can be more than an order of magnitude.

We thank Paz London for his assistance during the experiments.

---

- [1] R. H. Dicke, Phys. Rev. **89**, 472 (1953).
- [2] H. G. Robinson and C. E. Johnson, Applied Physics Letters **40**, 771 (1982).
- [3] D. Budker, L. Hollberg, D. F. Kimball, J. Kitching, S. Pustelny, and V. V. Yashchuk, Phys. Rev. A **71**, 012903 (2005).
- [4] N. Cyr, M. Tetu, and M. Breton, IEEE Transactions on Instrumentation and Measurement **42**, 640 (1993).
- [5] A. Nagel, C. Affolderbach, S. Knappe, and R. Wynands, Phys. Rev. A **61**, 012504 (1999).
- [6] J. Vanier, M. W. Levine, D. Janssen, and M. Delaney, Phys. Rev. A **67**, 065801 (2003).
- [7] M. Erhard and H. Helm, Phys. Rev. A **63**, 043813 (2001).
- [8] O. Firstenberg, M. Shuker, A. Ben-Kish, D. R. Fredkin, N. Davidson, and A. Ron (2007), quant-ph/0701008.
- [9] R. M. Camacho, C. J. Broadbent, I. Ali-Khan, and J. C. Howell, Physical Review Letters **98**, 043902 (2007).
- [10] T. Hong, Phys. Rev. Lett. **90**, 183901 (2003).
- [11] I. Friedler, G. Kurizki, O. Cohen, and M. Segev, Optics Letters **30**, 3374 (2005).
- [12] A. Andre, M. Bajcsy, A. S. Zibrov, and M. D. Lukin, Physical Review Letters **94**, 063902 (2005).
- [13] A. M. Akulshin, A. A. Celikov, and V. L. Velichansky, Optics Communications **84**, 139 (1991).
- [14] C. Y. Ye and A. S. Zibrov, Phys. Rev. A **65**, 023806

(2002).

[15] P. R. S. Carvalho, L. E. E. de Araujo, and J. W. R. Tabosa, Phys. Rev. A **70**, 063818 (2004).

[16] A. Nagel, S. Brandt, D. Meschede, and R. Wynands, Europhysics Letters (EPL) **48**, 385 (1999).

[17] M. Graf, E. Arimondo, E. S. Fry, D. E. Nikonov, G. G. Padmabandu, M. O. Scully, and S.-Y. Zhu, Phys. Rev. A **51**, 4030 (1995).

[18] K. E. Gibble and A. Gallagher, Phys. Rev. A **43**, 1366 (1991).

[19] R. Pugatch, M. Shuker, O. Firstenberg, A. Ron, and Davidson (2007), quant-ph/0701132.

[20] In this experiment we used an external-cavity diode laser instead of the VCSEL that appears in the figure.

[21] S. Knappe, V. Shah, P. D. D. Schwindt, L. Hollberg, J. Kitching, L.-A. Liew, and J. Moreland, Applied Physics Letters **85**, 1460 (2004).